THE JOURNAL OF BIOLOGICAL CHEMISTRY VOL. 285, NO. 2, pp. 1457–1467, January 8, 2010

In Vivo Stoichiometry of Shelterin Components*[S]

Received for publication, June 26, 2009, and in revised form, September 29, 2009 Published, JBC Papers in Press, October 28, 2009, DOI 10.1074/jbc.M109.038026

Kaori K. Takai, Sarah Hooper[1], Stephanie Blackwood[2], Rita Gandhi[3], and Titia de Lange[4]

From the Laboratory for Cell Biology and Genetics, The Rockefeller University, New York, New York 10065-6399

Human telomeres bind shelterin, the six-subunit protein complex that protects chromosome ends from the DNA damage response and regulates telomere length maintenance by telomerase. We used quantitative immunoblotting to determine the abundance and stoichiometry of the shelterin proteins in the chromatin-bound protein fraction of human cells. The abundance of shelterin components was similar in primary and transformed cells and was not correlated with telomere length. The duplex telomeric DNA binding factors in shelterin, TRF1 and TRF2, were sufficiently abundant to cover all telomeric DNA in cells with short telomeres. The TPP1·POT1 heterodimer was present 50–100 copies/telomere, which is in excess of its single-stranded telomeric DNA binding sites, indicating that some of the TPP1·POT1 in shelterin is not associated with the single-stranded telomeric DNA. TRF2 and Rap1 were present at 1:1 stoichiometry as were TPP1 and POT1. The abundance of TIN2 was sufficient to allow each TRF1 and TRF2 to bind to TIN2. Remarkably, TPP1 and POT1 were ~10-fold less abundant than their TIN2 partner in shelterin, raising the question of what limits the accumulation of TPP1·POT1 at telomeres. Finally, we report that a 10-fold reduction in TRF2 affects the regulation of telomere length but not the protection of telomeres in tumor cell lines.

Telomeres solve the two main problems associated with the organization of eukaryotic genetic information on linear chromosomes: that is, the end-replication problem and the end-protection problem. The end-replication problem is solved by the interaction of telomeres with telomerase, a telomere-specific reverse transcriptase that can replenish telomeric sequences lost during DNA replication (1). Mammalian telomeres solve the end-protection problem through their association with shelterin, a six-protein complex that specifically associates with telomeric DNA and represses both DNA damage signaling and double-strand break repair reactions at the chromosome ends (2).

Shelterin binds to the duplex telomeric TTAGGG repeat array through two related DNA-binding proteins, TRF1 and TRF2 (3–5). A third DNA binding factor in shelterin, POT1, binds to single-stranded TTAGGG repeats (6). A 50–400-nucleotide stretch of single-stranded DNA is found at the 3′ terminus of telomeres (7) or at a telomere-internal displacement loop (D loop) that is formed by strand-invasion of the 3′ overhang when telomeres are in the t-loop configuration (8). *In vitro*, POT1 can bind to TTAGGG repeats both at a 3′ end and at the non-terminal sites found in the D loop (9–12). The POT1 DNA binding activity is enhanced by its binding partner TPP1 (9–12). TPP1 also connects POT1 to TIN2, which binds to TRF1 and TRF2 (13–19). The sixth component of human shelterin, Rap1, interacts with TRF2 (20).

The view that the shelterin components can form a single six-subunit complex at telomeres has emerged from both the biochemical purification of the six-protein complex and studies of the protein-protein interaction network, including the finding that TIN2 can bind TRF1 and TRF2 simultaneously and the fact that immunoprecipitation of TRF1 brings down all other members of the complex (14–19, 21). In addition to the six-member complex, a five-member complex lacking TRF1 and a separate TRF2·Rap1 complex can be isolated from nuclear extracts, but it is unclear to what extent these subcomplexes are formed during the purification. For instance, the association of TRF2·Rap1 with the rest of shelterin is diminished in the high concentrations of salt required for the isolation of these chromatin-bound factors (17). The effects of loss of TRF1, TIN2, TRF2, POT1, and TPP1 on other shelterin components also suggest a more complex situation, consistent with the occurrence of separate TRF1·TIN2·TPP1·POT1 and TRF2·Rap1·TIN2·TPP1·POT1 complexes as well as the six-protein complex. In particular, deletion of TRF2 from mouse cells leads to nearly complete loss of Rap1 protein as determined by immunoblotting, immunofluorescence (IF),[5] and ChIP but only leads to a 2-fold reduction of the telomeric DNA signal in ChIPs with TIN2, TPP1, and POT1 (22, 23). Furthermore, the telomeric DNA signal in TRF1 ChIPs is not affected when TRF2 is deleted (23). Similarly, TRF1 remains associated with telomeres in human cells that overexpress a dominant negative allele of TRF2 (24, 25). These data indicate that TRF1 and TRF2 can bind to telomeres independently but do not address whether they normally do so.

Information on the type of complexes formed by the shelterin proteins is pertinent to attempts to understand how shelterin represses the DNA damage response at telomeres. In this regard, the repression of ATM signaling and inappropriate NHEJ (nonhomologous DNA end joining) at chromosome ends

* This work was supported, in whole or in part, by National Institutes of Health grants CA076027, GM09046, and AG016642 (to T. d. L.).

[S] The on-line version of this article (available at http://www.jbc.org) contains supplemental Figs. 1–6.

[1] Current address: Vanderbilt University Medical Center, 1211 Medical Center Dr., Nashville TN 37232.

[2] Current address: 40 Acres and A Mule Filmworks, 75 South Elliot Place, Brooklyn, NY 11217.

[3] Current address: Dupont Knowledge Centre, Genome Valley, Hydrabad 500 078, India.

[4] To whom correspondence should be addressed: The Rockefeller University, 1230 York Ave., New York, NY 10065-6399. Fax: 212-327-7147; E-mail: delange@mail.rockefeller.edu.

[5] The abbreviations used are: IF, immunofluorescence; TIF, telomere dysfunction-induced foci; ChIP, chromatin immunoprecipitation; PBS, phosphate-buffered saline; shRNA, short hairpin RNA; PD, population doubling.

is largely independent of POT1 proteins, whereas repression of ATR kinase signaling does not require TRF2 and Rap1 (23, 26–28). However, it is not known whether these separate functions reflect different aspects of one complex or reflect the presence of functionally distinct shelterin subcomplexes at telomeres. Similarly, the abundance and stoichiometry of shelterin subunits is relevant to the question of how telomere length homeostasis is achieved. According to the current "protein-counting" models for telomere-length homeostasis, the shortest telomeres in a cell are preferentially elongated by telomerase due to their diminished loading of shelterin, which acts as an inhibitor of telomerase-mediated telomere elongation (for review, see Ref. 29). Consistent with this model, inhibition of TRF1, TIN2, TPP1, and POT1 results in telomere elongation by telomerase *in vivo* (14–16, 25, 30), and POT1 has the ability to inhibit telomerase *in vitro* (31). According to the simplest version of the protein-counting model, the longer telomeres in a cell will contain more POT1 on the chromosome end, thereby blocking telomerase.

Quantitative analysis of the expression of the shelterin components has not been performed, and their stoichiometry is not known. This information is crucial to understanding the function of this complex and for future biochemical and structural analysis of reconstituted recombinant shelterin. We have determined the abundance of each of the shelterin subunits in human cells with short or long telomeres and established the effects of a 10-fold reduction in the most abundant shelterin component, TRF2, on telomere length regulation and telomere protection.

EXPERIMENTAL PROCEDURES

Cell Lines—HT1080, HTC75, HeLa1.2.11, and HeLaII cell lines were published previously. HeLa1.3 was derived from HeLa1.2.11, and HeLa204 was cloned from HeLaII by subcloning using cloning cylinders, and all human cell lines were genotyped with AmpFlST PCR analysis of polymorphic short tandem repeat loci. Mouse NIH3T3 cells and primary human fibroblasts (IMR90, MRC5, and WI38) were obtained from the ATCC. All cells lines were grown in Dulbecco's modified Eagle's medium supplemented with L-glutamine, penicillin-streptomycin, and nonessential amino acids and serum. HTC75 and HeLa cells were grown in 10% bovine calf serum (HyClone); for primary human cells, media contained 15% fetal bovine serum (Invitrogen).

Baculovirus-derived Proteins—All human shelterin proteins were produced in baculovirus using standard procedures. N-terminal His_6-tagged TRF1, TRF2, Rap1, and TIN2 proteins were cloned in pBacPac and reported previously (20, 32, 33). The 458-amino acids open reading frame of human TPP1 (starting with MAGSG) was endowed with a C-terminal His_6 tag and was cloned in pFastBacDual. His-tagged proteins were isolated from Hi5 insect cells on chelating Sepharose fast flow (GE Healthcare) nickel resin. Human POT1 with an N-terminal FLAG tag was cloned in pFBDM (34). For purification of FLAG-POT1, infected cells were harvested and lysed in 5 ml of cold lysis buffer (50 mM Tris, pH 7.4, 150 mM NaCl, 1% Triton X-100, 5 mM β-mercaptoethanol supplemented with Roche Applied Science protease inhibitor mixture) per 100 ml of cell culture. All subsequent steps were done at 4 °C. After incubation on ice for 10 min, the mixture was sonicated and cleared by centrifugation at 13,200 rpm for 20 min. The supernatant was incubated with M2 (FLAG antibody)-agarose beads (350-μl packed volume/100-ml cell culture) for 2 h on a nutator. Beads were prewashed 3 times in 50 mM Tris, pH 7.4, 150 mM NaCl. Beads were pelleted at 4000 rpm for 1 min and washed once with lysis buffer, once with lysis buffer with 0.5 M NaCl, and once with elution buffer without FLAG peptide (20 mM Tris-HCl, pH 8, 0.1 M KCl, 5 mM $MgCl_2$, 10% glycerol, 0.1% Tween 20, 5 mM β-mercaptoethanol, 0.2 mM phenylmethylsulfonyl fluoride). Protein was eluted in 3 steps of 400 μl of elution buffer with 160-μg/ml 3×FLAG peptide (Sigma) for 30 min nutating. Proteins were stored at −80 °C.

Immunoblotting—Asynchronously growing cells were trypsinized, resuspended with serum-containing media, and counted using a Coulter counter. After washing with phosphate-buffered saline (PBS), cells were suspended in 2× sample buffer (75 mM Tris-Cl, pH 6.8, 10% glycerol, 2% SDS, 0.05% bromphenol blue, 2.5% β-mercaptoethanol) at 10^4 cells/μl, heated to 100 °C for 5 min, and applied to 8 or 10% SDS-PAGE. Proteins were transferred to nitrocellulose membranes in transfer buffer (25 mM Tris, pH 8.3, 0.192 M glycine, 20% methanol). For POT1, guanidine renaturation was performed as described (25). Membranes were blocked with PBS, 0.5% Tween 20 with 10% nonfat dry milk at room temperature for 30 min and incubated with primary antibodies (rabbit polyclonal anti-hTRF1 antibody (#371), anti-hTRF2 antibody (#647), anti-hRap1 antibody (#765), anti-hTIN2 antibody (#864), anti-hTPP1 antibody (#1150), anti-hPOT1 antibody (#978), mouse monoclonal anti-γ-tubulin antibody (GTU88, Sigma), or anti-α-tubulin antibody (Sigma) at room temperature for 1 h or at 4 °C overnight followed by horseradish peroxidase-conjugated secondary antibodies (Amersham Biosciences) for 30 min. Signals were detected with ECL (Amersham Biosciences) and exposed to x-ray film.

Cell Fractionation—Cell fractionation was performed using the protocol of Méndez and Stillman (35). Cells were trypsinized, suspended in media containing serum, collected by centrifugation, and washed with PBS. All procedures were performed on ice. Cells were suspended in ice-cold buffer A (10 mM HEPES, pH 7.9, 10 mM KCl, 1.5 mM $MgCl_2$, 0.34 M sucrose, 10% glycerol, 1 mM dithiothreitol, 1 mM phenylmethylsulfonyl fluoride, and a protease inhibitor mixture). Triton X-100 as added to 0.1%, and cells were incubated for 10 min. The cytoplasmic fraction was collected by centrifugation at 1300 × *g* for 4 min. After washing with buffer A, the cell pellet was suspended in buffer B (3 mM, EDTA, 0.2 mM EGTA, 1 mM dithiothreitol, and the protease inhibitors described above) and incubated for 30 min. The lysate was fractionated to the supernatant (soluble nuclear fraction) and pellet (chromatin fraction) by centrifugation at 1700 × *g* for 4 min.

shRNAs—TRF2 shRNA were cloned in the pSUPERretro-puro vector. The sequences of the shRNA targets are as follows: sh1, 5′- CAGGAGCATGGTTCCTAATAATA-3′; sh2, 5′-AAG-CAGAAGTGGACTGTAGAAGA-3′; sh5, 5′-TCACAGGAG-CATGGTTCCTAATA-3′; sh8, 5′-AAAGACTTGGCATG-AACTGAAAC-3′; sh10, 5′-GTAGAACCTTCTCCTAGG-

AAATG-3′. The sequence of the Luciferase shRNA target is 5′-CGTACGCGGAATACTTCGA. The shRNA to POT1 (sh7) in pSUPERIOR retroviral vector was published previously (36). Retroviral infections were performed as described previously (37).

Telomere Length Analysis—For telomere length analysis, cells were harvested at the indicated PD, and DNA was isolated and digested with AluI and MboI. DNA was separated on a 0.7% agarose gel and transferred to a Hybond membrane for hybridization using an 800-bp telomeric DNA probe from pSP73Sty11 labeled with [CCCTAA]3-primed Klenow polymerase and [α-^{32}P]dCTP. Blots were exposed to a phosphorimaging screen and quantified telomeric DNA signals using ImageQuant. The rates of telomere shortening were calculated by linear regression. PD 0 was set at day 10 post-infection with the shRNA retroviruses.

Analysis of the Telomere Terminus—Telomere overhang analysis was performed as described previously (27). Signals were quantified, and the single-stranded telomeric signal (from probing of the native DNA) was normalized to total telomeric DNA signal (from probing of the denatured DNA) in the same lane. The normalized values were compared between samples. The 5′-terminal nucleotide was assayed as described previously (38). For each DNA sample, multiple ligation reactions were performed with individual C-telorettes (see below). EcoRI-digested genomic DNA (10 ng) was incubated in a 10-μl reaction mix (1× ligase buffer, 0.5 units of T4 ligase, 10^{-2}–10^{-5} μM concentrations of individual telorettes) at 35 °C for 12 h. Multiple PCR amplification reactions were performed (26 cycles of 95 °C for 15 s, 58 °C for 20 s, and 72 °C for 10 min) using 1 unit of Fail Safe enzyme mix (Epicenter), 12.5 μl of Fail Safe buffer H (2×, manufacturer), and 0.1 μM primers (XpYp E2 forward primer and Teltail reverse primer) in a final volume of 25 μl containing DNA at 200 pg/μl. Amplification products were resolved on a 0.5% agarose gel, denatured, transferred onto a positively charged nylon membrane (Zetaprobe; Bio-Rad), cross-linked with UV (Stratalinker), and hybridized with a subtelomeric probe (generated by PCR amplification using XpYpE2 and XpYpB2 and labeled by random priming). The membrane was exposed to a phosphorimaging screen and scanned by PhosphorImager (Amersham Biosciences).

Co-immunoprecipitation—Co-immunoprecipitation using HeLa1.3 expressing human POT1 or TIN2 was done as previously described (33). HeLa cells infected with retroviral vectors expressing FLAG-tagged POT1 or TIN2 were dislodged by flushing with cold PBS, collected by centrifugation, and lysed in ice-cold buffer (50 mM Tris-HCl, pH 7.4, 1 mM EDTA, 400 mM NaCl, 1% Triton X-100, 0.1% SDS, 1 mM dithiothreitol, 1 mM phenylmethylsulfonyl fluoride, and a protease inhibitor mixture). After 10 min on ice, an equal volume of ice-cold water was added and mixed thoroughly. The lysate was centrifuged at 14,000 rpm for 10 min, and the supernatant was used for immunoprecipitation. The prepared lysates were incubated with M2 FLAG mouse monoclonal antibody (Sigma) for 4 h at 4 °C while nutating. During the final hour, we added 30 μl (settled volume) of protein G-Sepharose beads (preblocked overnight with 10% bovine serum albumin in PBS) to each tube. The beads were washed three times with lysis buffer, and proteins were eluted with Laemmli loading buffer for analysis on SDS-PAGE.

Telomere Dysfunction-induced Foci (TIF) Analysis and IF/Fluorescence in Situ Hybridization—Telomeric DNA fluorescence *in situ* hybridization was combined with IF using a monoclonal mouse anti human 53BP1 antibody or TRF2 (Ab 647) using the protocol developed by Sedivy and co-workers (39) with the exception that a fluorescein isothiocyanate (FITC)-TelC (FITC-OO-CCCTAACCCTAACCCTAA, Applied BioSystems) probe was used to detect telomeric DNA. DNA was stained with 4,6-diamino-2-phenylindole.

RESULTS

Derivation of Cell Lines for This Study—We set out to determine the expression levels of shelterin components in tumor cell lines with different telomere lengths and in primary human fibroblasts. For this study we used four HeLa cell lines; HeLaI and HeLaII are previously described (referred to as HeLa-L and HeLa-S, respectively, in Rer 40) and differ in the length of their telomeres. HeLaI telomeres are >20 kb, whereas HeLaII telomeres are in the 4-kb range. HeLaI was subjected to successive rounds of subcloning in our laboratory to maintain a source of cells with uniform long telomeres. The successive subclones are called HeLa1.2, HeLa1.2.11, and HeLa1.3. The telomere lengths of the HeLa clones from the last round of subcloning are shown in supplemental Fig. 1*A*, which demonstrates the previously noted telomere length heterogeneity of HeLa subclones (41). This latest round of subcloning also yielded HeLa204, a cell line with telomeres in the 6-kb range. The telomere lengths of these new subclones are stable (supplemental Fig. 1*B* and data not shown). We executed genotypic analysis to ensure that the new HeLa cell lines as well as HeLa1.2.11 and HeLaII were indeed HeLa lines. The data showed that each carried identical alleles at 14 polymorphic loci (supplemental Fig. 1*C*), indicating that they are derived from the same individual.

A third tumor line used in this study is the HTC75 cell line, a subclone of the HT1080 fibrosarcoma cell line with short telomeres (30). This cell line is particularly relevant to telomere biology because it is the main cell line used for studies of telomere-length homeostasis. The primary human fibroblast strains, IMR90, WI-38, and MRC5 have been studied for their telomere biology extensively.

Development of a Method for Quantitative Assessment of TRF2—We first developed a technique for quantitative assessment of the shelterin components using TRF2 as a test case. To calibrate the TRF2 immunoblots, His-tagged TRF2 was purified from baculovirus-infected cells and used as a standard (Fig. 1*A*). The TRF2 concentration in the standard was determined by comparison to known quantities of bovine serum albumin and correcting for the number of Coomassie-reactive amino acids (Lys, His, Arg) in TRF2 and bovine serum albumin. TRF2 signals in Western blots of whole cell lysates were compared with the baculovirus-derived TRF2 standard to estimate the number of TRF2 molecules per cell (Fig. 1, *B* and *C*). The assay appeared robust in multiple independent experiments for TRF2 and the other shelterin components (see Table 1). A similar approach was used by Wu and Pollard to determine protein abundance in *Schizosaccharomyces pombe* (42).

The cell lysates were normalized based on cell number rather than a control protein (*e.g.* tubulin) because of uncertainties associated with the expression level of any protein in these cells. Cell lysates were always derived from logarithmically growing cells to minimize variations due to cell cycle stage.

For the quantification of TRF2, both TRF2 species were taken into account. Unlike baculovirus-derived TRF2, TRF2 from human cells is represented in immunoblots by two closely migrating bands (Fig. 1*B*). Both bands are derived from the TRF2 mRNA because both disappear upon TRF2 knockdown with shRNA (see Fig. 4). The difference between these two forms of TRF2 is not known; their relative abundance varies from cell line to cell line. When both forms of TRF2 were taken into account, all cell lines examined contained on the order of $0.5–1 \times 10^5$ molecules of TRF2 per cell (Fig. 1*C* and Table 1). If all TRF2 is bound to telomeric DNA, the chromosome ends are predicted to contain hundreds of copies of TRF2. The abundance of TRF2 was not lower in the cells with short telomeres (HeLaII, HeLa204, HTC75, IMR90, and MRC5 cells, Fig. 1*C*, Fig. 2, and data not shown) compared with HeLa cells with long telomeres. The abundance of TRF2 in the cells with short telomeres could potentially represent a 10-fold higher density of loading of TRF2 per kb of telomeric DNA. However, indirect IF analysis of MRC5, IMR90, and HTC75 cells performed in parallel with HeLa1.3 cells showed more TRF2 staining throughout the nucleus in the cells with short telomeres (supplemental Fig. 2 and data not shown). Treatment with shRNA showed that this non-telomeric signal is derived from TRF2 (supplemental Fig. 2). Therefore, the total amount of TRF2 per cell may, not reflect the loading of TRF2 per telomere.

Quantitative Analysis of all Six Shelterin Components—Having established a procedure to quantify the expression level of TRF2 in different cell lines, we applied the same approach to the other shelterin components. For each shelterin component, immunoblots were calibrated using purified baculovirus-derived proteins for which the concentration was determined as detailed above for TRF2. The shelterin components were analyzed in whole cell lysates of HeLa1.3 and HTC75 cells. Each protein was detected with affinity-purified antibodies developed in our laboratory for which the correct band(s) in whole cell lysates were identified based on prior purification efforts and/or shRNA knockdown results (Refs. 3, 5, 14, 17, 25, 36 and see below). For the TPP1 antibody, we identified the relevant species based on their co-immunoprecipitation with TIN2 and POT1 (supplemental Fig. 3). These experiments identify TPP1 as a set of three bands migrating around 50 kDa in 8% SDS-polyacrylamide gels. As for TRF2, all three bands were taken into account in the analysis of the abundance of TPP1. Finally, our antibody to POT1 detects two versions of this protein, full-length POT1 and POT1–55, which lacks one of the two OB-folds (Ref. 36 and data not shown). In all cell lines tested, POT1–55 was 3-fold less abundant than full-length POT1, and the two proteins behaved the

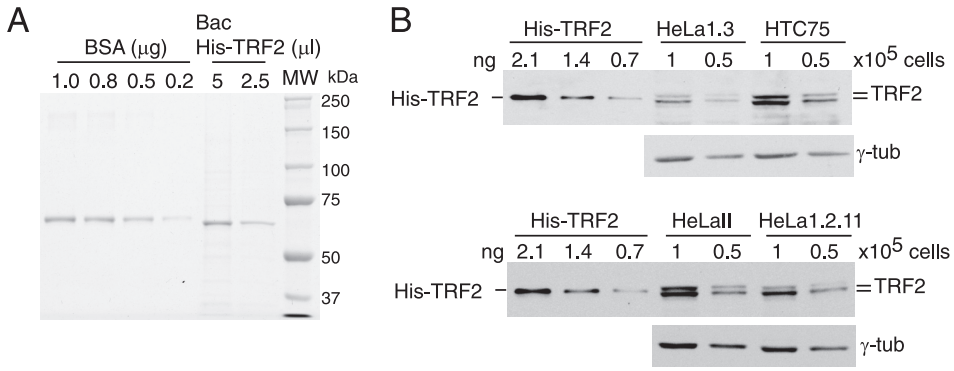

C

telomere length	23 kb		4 kb		9 kb
cell line:	HeLa1.3	HeLa1.2.11	HTC75	HeLaII	IMR90
chromosomes/cell	71	76[a]	70	76[a]	46
TRF2 molecules/cell (X10^3)	60	90	120	140	50

[a] ref. 59

FIGURE 1. **Method for quantification of TRF2.** *A*, shown is quantification of the baculovirus (*Bac*)-derived His-TRF2 standard. *BSA*, bovine serum albumin. *B*, shown is quantitative immunoblotting for TRF2 in whole cell lysates of the indicated cell lines using calibration with the baculovirus-derived His-TRF2 as a standard. *C*, shown is the calculated abundance of TRF2 in the cell lines analyzed in *B*.

TABLE 1

Abundance of shelterin components determined by quantitative immunoblotting

The number of molecules indicated are the averages of 3 or more experiments (S.D. are below 10% of values). The values are corrected by the detection factor shown in supplemental Fig. 4.

	HeLa1.3[a]			HTC75[b]		
	Per cell (×10^3)	Chromatin- bound (×10^3)	Per telomere[c]	Per cell (×10^3)	Chromatin- bound (×10^3)	Per telomere[c]
TRF1	40	40	270	25	25	180
TRF2	60	60	420	120	120	860
Rap1	190	65	440	370	150	1060
TIN2	125	100	720	150	120	840
TPP1	20	27	95	22	8	50
POT1	12	9	65	16	7	50

[a] Average chromosome number, 2n = 71; telomere length, ~23 kb.
[b] Average chromosome number, 2n = 70; telomere length, ~4 kb.
[c] Assuming all chromatin-bound protein is associated with telomeres.

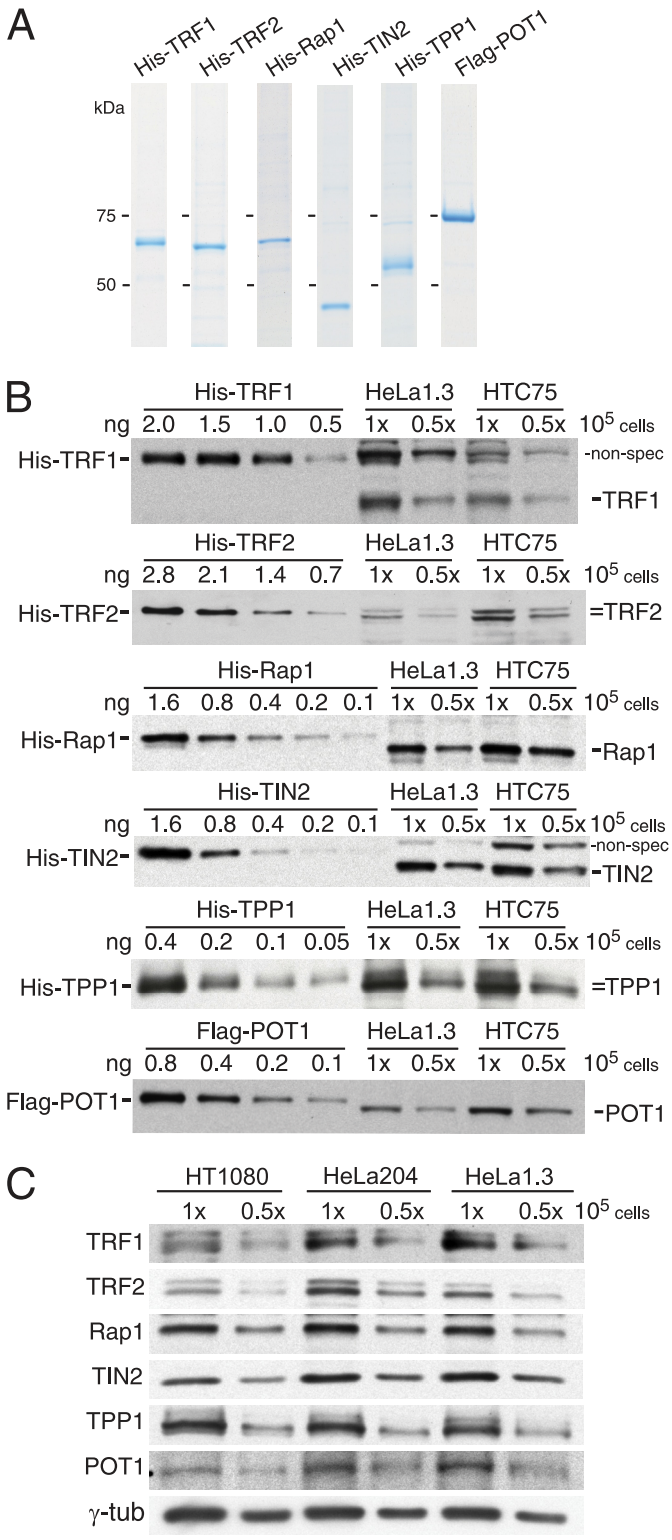

FIGURE 2. **Quantitative analysis of the six shelterin components.** *A*, shown are baculovirus-derived shelterin components used to calibrate the immunoblots. *B*, shown is quantitative immunoblotting for each of the shelterin components in whole cell lysates of the indicated cell lines using calibration with the baculovirus-derived proteins in *A* as a standard. The concentrations of the baculovirus-derived proteins were determined as in Fig. 1*A*. Antibodies used were: TRF1, 371; TRF2, 647; Rap1, 765; TIN2, 864; TPP1, 1150; POT1, 978. Immunoblotting for POT1 was done using guanidine renaturation. *C*, comparison of the abundance of shelterin components in two additional cell lines with short telomeres (HT1080 and HeLa204) to HeLa1.3.

same in cell fractionation experiments (data not shown), consistent with the previous finding that both versions of POT1 are capable of localizing to telomeres (36). Both forms of POT1 were included in the quantification.

As an additional control for the quantitative assessment of shelterin proteins in cell lysates, we tested whether the presence of the proteins in a lane containing the complex mixture of proteins present in a cell lysate affects the quantification. To this end, purified recombinant protein was mixed in with known quantities of cell lysate, and the immunoblot signals were compared with the recombinant protein fractionated by itself or in the presence of bovine serum albumin (supplemental Fig. 4). These controls indicated that the immunoblotting signal of the known quantity of recombinant protein was enhanced in the lysate. This increase in detection was not observed for Rap1, but it occurred for all the other components. The increase ranged from 2 to 4-fold. We, therefore, incorporated a detection correction factor in the quantification of each of the shelterin components to account for this difference.

The results for HeLa1.3 cells showed that TRF1, TRF2, Rap1, and TIN2 are all abundant, present at 30–200 thousand copies per cell (Fig. 2; Table 1). The levels of TRF1 and TIN2 were very similar in HeLa1.3 and HTC75 cells, whereas both Rap1 and TRF2 were more abundant in HTC75 cells. This concordance between TRF2 and Rap1 levels is consistent with observations in mouse cells where Rap1 depends on TRF2 for its stability (26).

Notably, TPP1 and POT1 were significantly less abundant than the other shelterin components, both present at 20,000 molecules per cell in HeLa1.3 and HTC75 cells (Fig. 2; Table 1). POT1 and TPP1 were also significantly less abundant than TRF1·TRF2·Rap1·TIN2 in primary human fibroblasts (data not shown).

We verified that HTC75 cells were not an exception with regard to shelterin abundance by comparing both HT1080 cells (the HTC75 parental cell line with short telomeres) and HeLa204 (short telomeres) with HeLa1.3 (long telomeres) (Fig. 2*C*). The analysis showed that there is no obvious correlation between the abundance of shelterin components and average telomere length.

We next asked what fraction of each of the shelterin proteins was chromatin-bound by fractionating HeLa1.3 and HTC75 cells (Fig. 3). Most of TRF1 and TRF2 were found to be chromatin-bound with no detectable protein in the soluble fractions. In contrast, a substantial fraction of Rap1, TIN2, TPP1, and POT1 was recovered in the soluble fractions of HeLa1.3, HeLa204, and HTC75 cells (Fig. 3, *A* and *B*, and data not shown).

Making the assumption that the chromatin-bound shelterin proteins are associated with telomeric DNA, the quantitative findings indicate that each telomere may contain as little as 50–100 molecules of POT1 and TPP1 (Table 1). The other components of shelterin are much more abundant (Table 1). If all chromatin-bound shelterin is actually associated with telomeres, the quantification also predicts that the HeLa1.3 cells with telomeres that are five times longer than those of HTC75 cells or HeLa204 cells do not contain five times more shelterin (Table 1 and Fig. 2*C*).

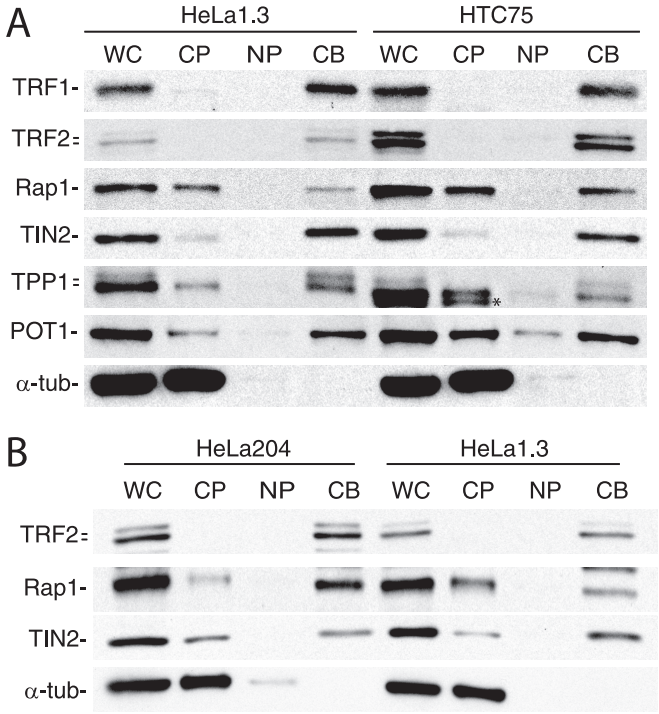

FIGURE 3. **Determination of the chromatin-bound and soluble fractions of the shelterin components.** *A* and *B*, the indicated cell lines were fractionated as described under "Experimental Procedures," and equal fractions of the whole cell lysate (*WC*), cytoplasmic proteins (*CP*), nucleoplasmic proteins (*NP*), and the insoluble nuclear fraction, referred to as chromatin-bound proteins (*CB*), were analyzed by immunoblotting. α-Tubulin (*α-tub*) was used as a control for cytoplasmic proteins. Antibodies are as in Fig. 2.

Quantification of the chromatin-bound proteins informs on the potential stoichiometry of the shelterin components at telomeres (Table 1). The stoichiometry of TRF2 to Rap1 is in the range of 1:1, which is in good agreement with the approximately equal silver-staining for TRF2 and Rap1 in the purified endogenous chromatin-bound TRF2 complex (43). Thus, each TRF2 dimer appears to be associated with two Rap1 molecules. TRF1 is 2–4-fold less abundant than the TRF2·Rap1 heterodimer, suggesting that TRF1 is a substoichiometric component. The abundance of TIN2 is sufficient to allow binding of one TIN2 molecule to each copy of TRF1 and TRF2 in the chromatin-bound fraction. TPP1 and POT1 are present at a roughly 1:1 stoichiometry, but the abundance of this heterodimer is ~10-fold lower than TIN2, the TPP1 interaction site in shelterin.

10-Fold Knockdown of TRF2 Affects Rap1 but Not TRF1, TIN2, TPP1, or POT1—A 10-fold reduction in the level of human POT1 results in a telomere deprotection phenotype (36). Given that cells contain 5–10-fold more TRF2 than POT1, we wished to establish how a 10-fold reduction in TRF2 is tolerated. We tested 5 shRNAs directed against TRF2, 2 of which (sh1 and sh5) resulted in a 10-fold reduction of the TRF2 protein levels, as determined based on quantitative immunoblot analysis of HTC75 cells (Fig. 4*A*). This level of knockdown was also achieved in HeLa cells and primary human fibroblasts (IMR90 and WI38) (Fig. 4*C*). The reduction of TRF2 levels led to an obvious loss of TRF2 from the telomeres as deduced from IF analysis (Fig. 4*B*, supplemental Fig. 2). In contrast, TRF1 remained associated with telomeres as deduced from IF (supplemental Fig. 2 and data not shown), and the levels of TRF1, TIN2, TPP1, and POT1 appeared unaltered based on immunoblotting (Fig. 4*C*). Furthermore, the amount of TRF1, TIN2, TPP1, and POT1 recovered in the chromatin-bound fraction was unaltered (Fig. 4*D*).

Whereas TRF2 shRNAs had no effect on TRF1, TIN2, TPP1, and POT1, the diminished TRF2 levels did affect Rap1. Although the overall level of Rap1 was only moderately diminished (Fig. 4*C*), Rap1 was severely depleted from the chromatin-bound protein fraction (Fig. 4*D*), consistent with its dependence on TRF2 for telomere binding. However, this fraction of Rap1 constitutes only ~50% of the total Rap1 protein, with the remainder fractionating with cytoplasmic proteins. The cytoplasmic fraction of Rap1 was not affected by TRF2 levels and may not be associated with TRF2 as TRF2 is mainly present in the chromatin-bound fraction (Figs. 3 and 4*D*). The partial depletion of Rap1 upon TRF2 knockdown contrasts the situation in mouse cells where deletion of TRF2 destabilizes most Rap1 (26). Interestingly, the majority of mouse Rap1 fractionates together with TRF2 to the chromatin-bound fraction (supplemental Fig. 5). Thus, whereas most mouse Rap1 appears dependent on TRF2 and is chromatin-bound, 50% of the human Rap1 is recovered in the cytoplasmic fraction and is unaffected by TRF2 levels. This difference is yet another example of distinctions between the shelterin complex in human and mouse cells (27, 44, 45).

Reduction in TRF2 Levels Affects Primary Human Cells—Three primary human fibroblast strains (IMR90, WI38, and MRC5) showed a mild proliferation defect when TRF2 was knocked down by 10-fold (Fig. 5, *A* and *B*), although there was no obvious effect on the rate of telomere shortening (Fig. 5, *C* and *D*). The cultures contained cells with a senescent morphology that stained positive for the senescence-associated β-galactosidase (Fig. 5*E* and data not shown). Upon prolonged culturing, the TRF2 levels in the fibroblasts increased, consistent with a selection against cells with the lowest TRF2 levels (Fig. 5*A*).

TRF2 knockdown induced 53BP1 TIFs in a small fraction (<10%) of the cells (Fig. 5, *F* and *H*). As a positive control, parallel knockdown of POT1 resulted in a strong TIF response in the cells (Fig. 5, *F* and *H*) (36). However, the TRF2 knockdown cells did show a significant number of very large 53BP1 foci that are reminiscent of the senescence DNA damage foci (46) previously noted in human cells undergoing replicative senescence (Fig. 5, *G* and *H*). These foci did not co-localize with telomeric DNA and may represent telomeres that have been extensively shortened and have lost their ability to protect chromosome ends under conditions of limiting TRF2.

No Overt Telomere Deprotection in Tumor Cell Lines with Reduced TRF2 Levels—In contrast to the primary fibroblasts, the HeLa and HTC75 cells with a 10-fold reduced TRF2 level did not show overt signs of telomere deprotection (Figs. 5 and 6). Their rate of proliferation was unaffected by TRF2 knockdown (Fig. 6*A*), and the cells did not contain a significant level of TIFs (Figs. 5*H* and 6*B*). The tumor cell lines with diminished TRF2 levels did show large 53BP1 senescence DNA damage-like foci, similar to what was observed in primary fibroblasts (Fig. 5*H*). It is possible that these foci represent sites of secondary damage caused by inhibition of TRF2, although HeLa and

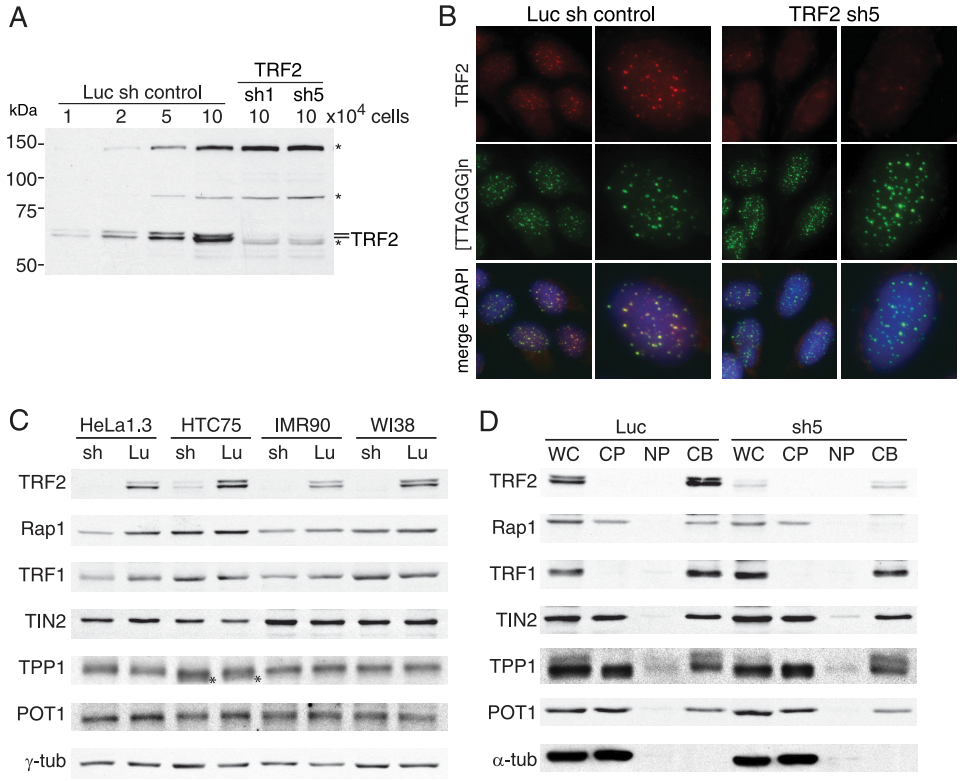

FIGURE 4. **Effect of shRNA-mediated knockdown of TRF2 on other shelterin components.** *A*, shown is quantitative immunoblotting to determine the reduction of TRF2 expression in cells (HTC75) infected with retroviruses carrying shRNAs 1 and 5 compared with the luciferase (*Luc*) shRNA control. *B*, IF for TRF2 (*red*) at telomeres detected by fluorescence *in situ* hybridization (*green*) in HeLa1.3 cells expressing the luciferase control or sh5 to TRF2 is shown. *DAPI*, 4,6-diamino-2-phenylindole, *C*, levels of all shelterin components in whole cell lysates of the indicated cells infected with sh5 to TRF2 or the luciferase control (*Lu*) are shown. γ-Tubulin (γ-*tub*) serves as the loading control. *D*, shown is the effect of TRF2 knockdown on soluble and chromatin-bound shelterin components. HTC75 cells infected with the luciferase control of sh5 were fractionated as described in Fig. 3, and equal cell equivalents of the fractions were analyzed by immunoblotting for the presence of shelterin components. *WC*, whole cell lysate; *CP*, cytoplasmic proteins; *NP*, nucleoplasmic proteins; CB, chromatin-bound proteins.

HTC75 cells did not show telomere fusions (<1 fusion per 1000 chromosomes) when TRF2 was knocked down. Consistent with the idea that HTC75 cells tolerate the reduced levels of TRF2, the level of TRF2 remained low over 100 PD (Fig. 6*C*). Thus, most telomeres in tumor cells retain the ability to repress the telomere DNA damage response despite their 10-fold lower level of TRF2.

TRF2 Knockdown Induces Telomere Elongation—In three independent experiments, the telomeres of HTC75 cells infected with the TRF2 shRNAs (sh1 and sh5) showed gradual and progressive elongation (Fig. 6, *D* and *E*). We have not been able to determine whether the telomere length phenotype is a result of depletion of TRF2 or Rap1 (or both) because extensive attempts to lower Rap1 levels by shRNA-mediated depletion were unsuccessful, possibly because Rap1 is synthesized in excess, and the Rap1 levels in the cell are determined by the expression of TRF2. However, a study by Songyang and co-workers (47) showed that diminished Rap1 levels could lead to telomere elongation.

In contrast to the effect on the length of the double-stranded telomeric region, TRF2 knockdown did not affect the structure of the telomere terminus, which has two characteristics; they are a 3′ overhang of TTAGGG repeats and a 5′ terminus with the sequence ATC-5′ (38). Quantitative assessment of the relative abundance of single-stranded TTAGGG repeats indicated that a 10-fold reduction in TRF2 levels did not affect this parameter (supplemental Fig. 6, *A* and *B*). In addition, STELA assays of HTC75 cells showed that the majority of telomeres ended on the sequence ATC-5′ and that TRF2 knockdown did not alter this pattern (supplemental Fig. 6, *C* and *D*).

DISCUSSION

In this study we have aimed to determine the stoichiometry of the shelterin components *in vivo*. Although results represent rough estimates rather than precise measurements, several noteworthy aspects of the shelterin complex were revealed. The stoichiometry within shelterin is such that each copy of TRF1 and TRF2 dimers can bind to a copy of TIN2. In addition, each TRF2 is likely to be associated with one copy of Rap1. We do not know whether all the TRF1·TIN2 and TRF2·TIN2·Rap1 complexes are connected to each other, but it is clear from the data that TRF1 and TRF2 are not equally abundant. TRF1 is substoichiometric, making it likely that there are TRF2·TIN2·Rap1 complexes that lack TRF1. TPP1 and POT1 are present at roughly a 1:1 stoichiometry, consistent with their forming a heterodimer (49) and the dependence of POT1 on TPP1 for its stability (23). The lower abundance of POT1 and TPP1 is in agreement with much greater ease of IF detection of TRF1, TRF2, TIN2, and Rap1 at telomeres than TPP1 or POT1. The substoichiometric presence of TPP1 in the shelterin complex argues against the idea that TPP1 is required to stabilize the TIN2·TRF1·TRF2 interactions as much of the TIN2·TRF1·TRF2 is predicted to lack an association with TPP1 (21).

The finding that TPP1·POT1 are much less abundant at telomeres than TIN2 raises the question of what limits their presence telomeres. Expression of POT1 from a strong exogenous promoter does not increase the abundance of this protein in cells (25), indicating that most POT1 is degraded. In mouse cells, co-expression of TPP1 stabilizes POT1 and leads to its greater accumulation at telomeres (23). Thus, it is likely that POT1 loading is dictated by the level of TPP1 at telomeres. Therefore, it will be important to understand how the accumulation of TPP1 at telomeres is regulated.

The results show that the double-stranded DNA binding factors in shelterin, TRF1 and TRF2, as well as their interacting

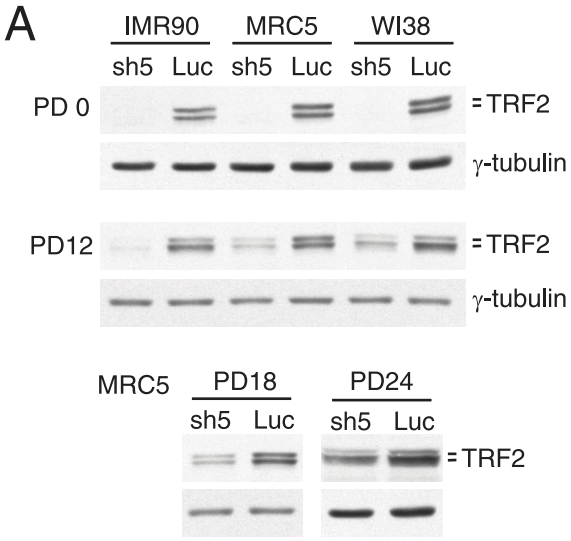

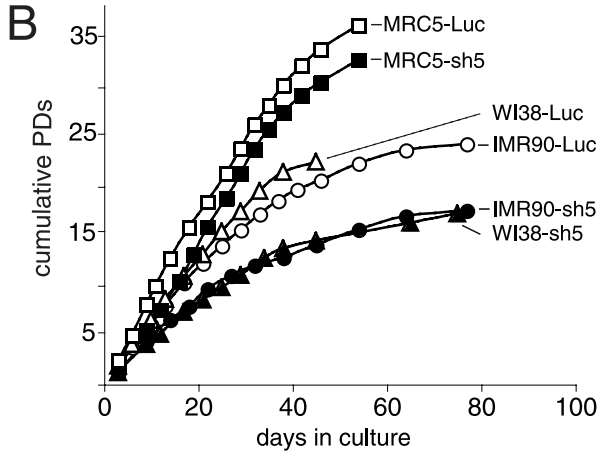

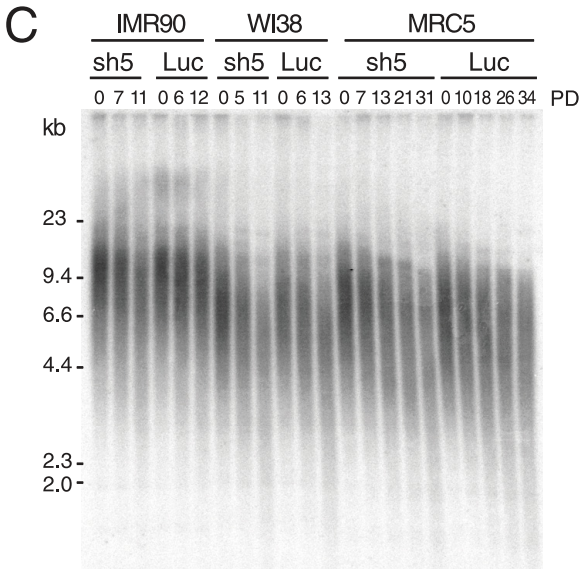

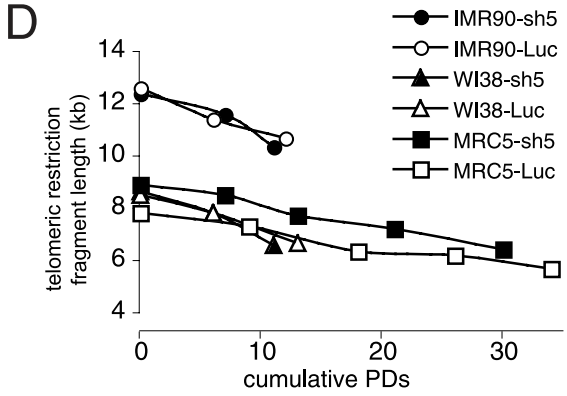

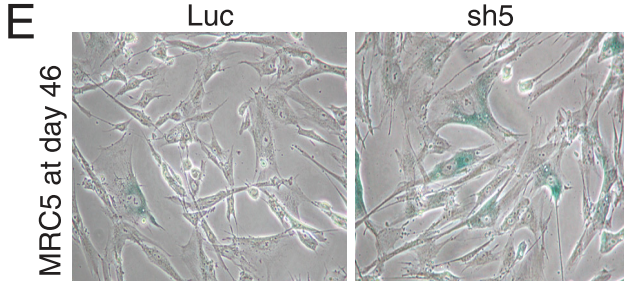

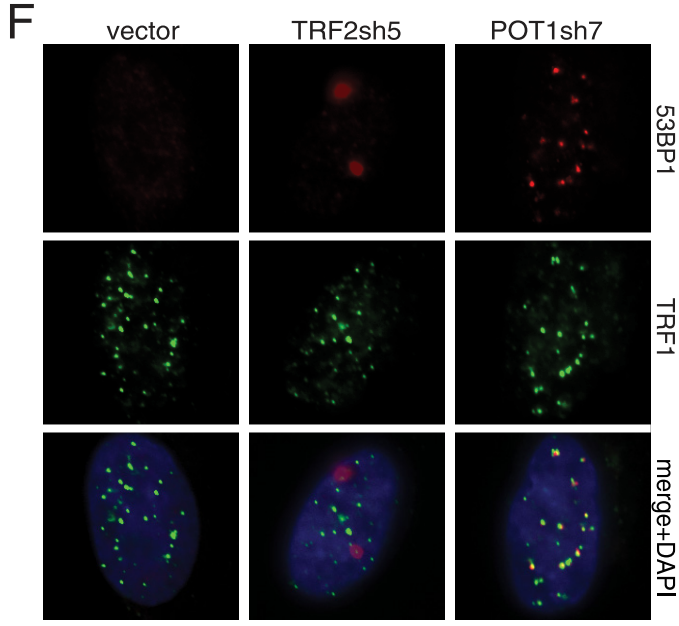

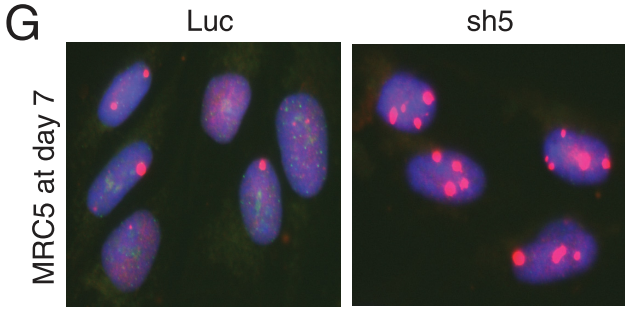

H

	% cells >5 TIFs (n)		% cells >3 large foci (n)	
	MRC5	HeLa1.3	MRC5	HeLa1.3
vector	<1 (276)	<1 (362)	6 (169)	3 (175)
TRF2sh5	7 (216)	3 (718)	19(159)	17 (184)
POT1sh7	33 (311)	22 (162)	<1 (148)	4 (139)

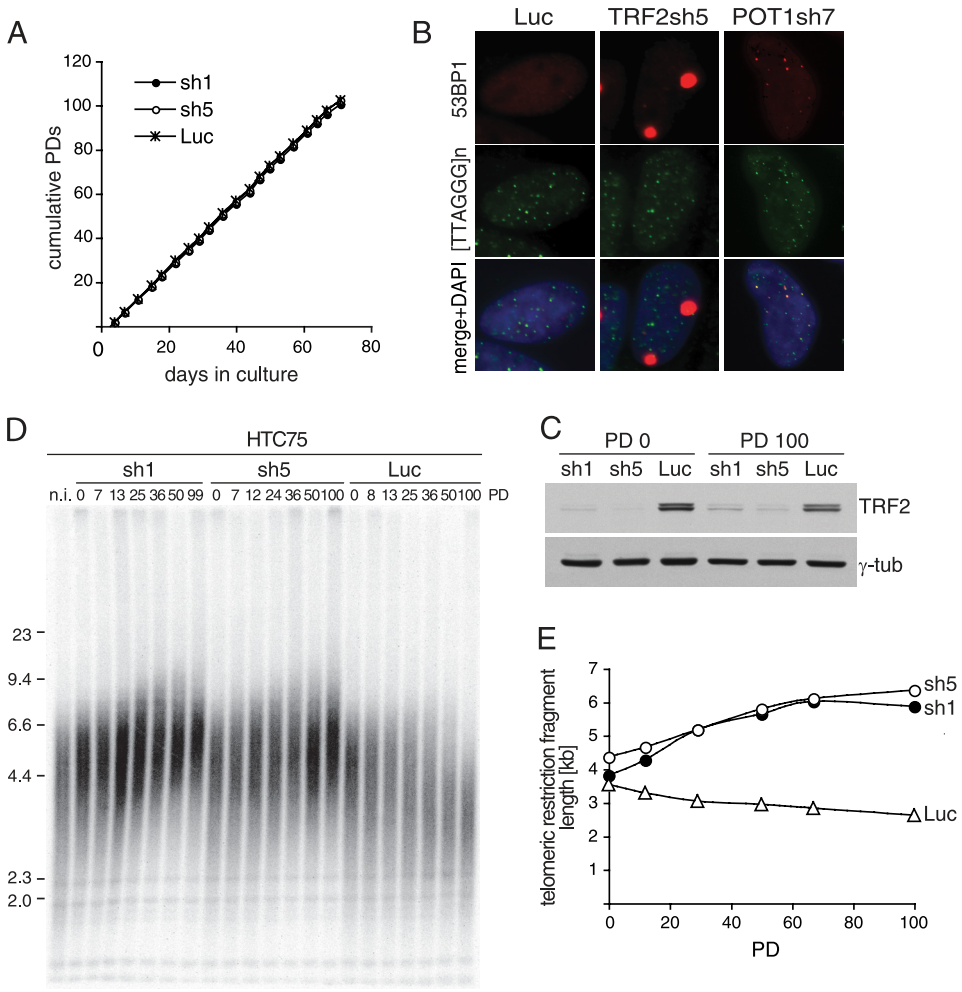

FIGURE 6. **Knockdown of TRF2 affects telomere length homeostasis but not telomere protection.** *A*, shown is a graph representing proliferation of HTC75 cells expressing the indicated shRNAs to TRF2 (sh1 and 5) or the luciferase (*Luc*) control. *B*, the absence of overt TIF phenotype in HeLa1.3 is shown. *C*, shown are immunoblots for TRF2 levels in whole cell lysates of HTC75 cells expressing the indicated shRNAs at early and late PD. γ-*tub*, γ-tubulin. *D*, shown is a genomic blot for telomeric restriction fragments in shRNA-treated HTC75 cells at the indicated PD. M_r markers are in kb. *E*, graphic representation of a second independent experiment is shown in which telomere length changes were recorded in HTC75 cells treated with sh1 or sh5 to TRF2. Methods were as *D*.

partners can be very abundant compared with the available TRF1/2 binding sites. HTC75 cells and other cells with relatively short telomeres (5 kb or shorter) contain sufficient TRF1 and TRF2 to provide every telomere with a thousand copies of these DNA binding factors. Given that each TRF1 or TRF2 dimer can associate with 2.5 copies of the TTAGGG repeat, this loading would have the potential to cover 7.5 kb of TTAGGG repeats, in excess of the available telomeric DNA. In agreement, IF analysis suggests that some of the TRF2 in these cells is not located at telomeres. As most of TRF2 is chromatin-bound, it will be of interest to determine whether this non-telomeric TRF2 (and perhaps TRF1) is associated with chromosome-internal TTAGGG sequences or bound to chromatin through non-specific interactions. It may be useful to perform ChIP-sequencing analysis of TRF1- and TRF2-associated DNA to determine whether there are chromosome internal binding sites for these proteins (and their associated factors) and, if so, what they represent.

The abundance of TRF2, TRF1, and their interacting partners TIN2 and Rap1 at telomeres provides a plethora of binding sites for shelterin accessory factors, many of which are thought to be linked to a specific docking site in the TRFH domains (48). Thus, it is possible that many different shelterin accessory factors are simultaneously bound to telomeres.

The loading of TRF1 and TRF2 on the long telomeres of HeLa1.3 cells is potentially less than in HTC75 and HeLa204 cells. HeLa1.3 cells only contain sufficient TRF1 and TRF2 to cover 10–20% of the telomeric DNA. Despite this diminished loading density, these long telomeres also contain hundreds of copies of TRF1·TRF2·Rap1·TIN2, thus potentially providing extensive interaction surfaces for shelterin accessory factors. We consider it likely that the different loading density of TRF1 and TRF2 on short and long telomeres is responsible for the previously noted difference in the nucleosomal organization of the telomeres as detected by micrococcal nuclease experiments (40).

TPP1·POT1 heterodimer, which associates with the sequence TTAGGGTTAG, is present in excess of its binding sites regardless of telomere length. There are an estimated 50–100 copies of TPP1·POT1 per telomere, sufficient to cover 500–1000 nucleotides of single-stranded DNA at each telomere. The single-stranded telomeric DNA ranges in length but is typically 50–100 nucleotides and rarely larger than 400 nucleotides. Therefore, a fraction of the telomere-bound TPP1·POT1 may not be associated with single-stranded DNA.

FIGURE 5. **Knockdown of TRF2 results in premature senescence in primary fibroblasts.** *A*, immunoblots of TRF2 levels in the indicated primary fibroblasts infected with TRF2 sh5 or the luciferase (*Luc*) controls are shown. TRF2 levels were analyzed at the indicated PDs. *B*, shown are growth curves of the cells described in *A*. PD 0 is set at day 10 after infection. *C*, shown is a genomic blot of telomeric restriction fragments in the cells described in *A* at the indicated PDs. M_r values are indicated in kb. *D*, shown is a graph displaying the length of the telomeric restriction fragments as a function of PD for the cells described in *A*. *E*, photographs of MRC5 expressing the indicated shRNAs at day 46 in *B* are shown. Cells were stained for senescence-associated β-galactosidase activity. *F*, shown is IF for 53BP1 (*red*) combined with TRF1 (*green*) on WI38 cells at day 10 after infection with the indicated shRNAs. The *bottom images* show a merge of the top two images with 4,6-diamino-2-phenylindole stain for DNA. *G*, example of large, non-telomeric 53BP1 foci induced by TRF2sh5 in MRC5 cells (day 7). *H*, a table enumerating the occurrence of TIFs and large, non-telomeric 53BP1 foci in MRC5 and HeLa1.3 treated with the indicated shRNAs is shown.

The quantitative assessment of the shelterin components is relevant to the analysis of telomeres by ChIP. ChIP with antibodies to each of the shelterin components on HeLa1.2.11 and HeLaII (long and short telomeres, respectively) yielded the same fraction of the telomeric DNA despite the vast difference in telomere length (25). For instance, TRF1 antibodies brought down 16 and 14% of the telomeric sequences in HeLaII and HeLa1.2.11, respectively. Our original interpretation of those data were that long telomeres and short telomeres have the same density of loading of the shelterin components. Our current data leads us to question this interpretation as the quantitative assessment suggests a much more sparse loading of shelterin on longer telomeres. ChIPs are done after shearing the DNA to an average size of 1 kb. We estimate that HeLa1.2.11 (like HeLa1.3) will contain ~5 dimers of TRF1 per kb, whereas HeLaII (like HTC75) may have as much as ~10–20 dimers of TRF1 per kb. In both cases there is likely to be sufficient TRF1 for antibody engagement even if the cross-linking of TRF1 to the DNA is not 100% efficient. Based on these data, we suspect that ChIP with shelterin proteins does not accurately report on changes in protein occupancy, although it does inform on the presence or absence of a particular factor. For instance, deletion of TRF2 from mouse cells abrogates the ChIP signals obtained with TRF2 or Rap1 (23). However, a dominant negative allele of TRF2, which reduced the TRF2 ChIP efficiency by 2-fold (25), probably removed much more than half of the TRF2 from the telomeres. This dominant negative allele resulted in an extensive DNA damage response involving most telomeres (50), which according to the current data requires loss of more than 90% of TRF2. Thus, the interpretation of ChIP data on changes in shelterin occupancy at telomeres may not be straightforward.

Implications for the Protein-counting Model of Telomere Length Control—The current model for telomere length regulation is that the telomeric DNA recruits a negative regulator of the telomerase pathway (29). According to this model, the shortest telomere in a cell has a greater chance of being elongated because it will recruit less of the negative regulator. In the mammalian version of this protein-counting model (51), the shortest telomere would carry less of one or more shelterin components that inhibit telomerase action. Previous experiments involving dominant negative alleles and shRNA knockdown have shown that TRF1, TIN2, Rap1, POT1, and TPP1 behave as such negative regulators of telomere elongation by telomerase (for review, see Ref. 29). Furthermore, overexpression and tethering experiments have confirmed that increased loading of TRF1 blocks telomere elongation by telomerase (52). Our current data now extend this analysis to inhibition of TRF2, which was previously not feasible due to the lethal effects of inactivation of TRF2 with a dominant negative allele.

The observation that cells with short telomeres contain more shelterin than cells with long telomeres is not in disagreement with the proposed role of shelterin in telomere length homeostasis. Although we assessed the overall level of shelterin, our data do not refute the idea that an abnormally short telomere in a cell will contain less shelterin than the other telomeres and, therefore, would be a preferred substrate for telomerase. In fact, the higher level of shelterin in HTC75 cells, compared with the HeLa cells with longer telomeres, could explain why HTC75 cells can maintain their telomeres at a stable short setting despite their high telomerase activity.

Within the context of the protein-counting model, POT1 has been ascribed a special role because it is the best candidate protein to act as the direct inhibitor of telomerase (11, 14, 25, 31, 53). Knockdown of POT1 or inhibition of its recruitment by TPP1 induces telomere elongation. Importantly, the DNA binding domain of POT1 is required for telomere length homeostasis, and *in vitro* experiments attest to the ability of POT1 to block the access of telomerase to the 3′ end of a telomeric substrate (31), although this inhibitory activity of POT1 is dependent on where it binds on the 3′ overhang (11, 54). In this regard our finding that TPP1 and POT1 are underrepresented on telomeres in comparison to their binding partner, TIN2, is pertinent. This finding argues against the simplest scenario for the protein-counting model wherein the length of the telomere, via the binding of TRF1·TRF2 and TIN2, is translated into greater loading of TPP1·POT1. In other words, TPP1·POT1 is not a good candidate for the proteins that are counted in the protein-counting model in which telomere length is gauged based on the number of associated telomere binding factors. The actual mechanism that allows cells to identify an abnormally short telomere in a cell remains to be illuminated. In addition, it needs to be clarified how the counting mechanism results in the inhibition of the telomerase by POT1 in a manner that is independent of the number of POT1 molecules loaded on the telomere. One possibility is that telomere-length homeostasis involves an as yet unknown modification of POT1 or its interacting factors.

Acknowledgments—We thank Dirk Hockemeyer, Jill Donigian, and Hiro Takai for technical advice, Imre Berger and Tim Richmond for pFBDM, Jan-Peter Daniels for the TPP1 baculovirus, and Agnel Sfeir for comments on this work. We also thank The Rockefeller University Genomics Research Center for service.

REFERENCES

1. Greider, C. W., and Blackburn, E. H. (1985) *Cell* **43,** 405–413
2. Palm, W., and de Lange, T. (2008) *Annu. Rev. Genet.* **42,** 301–334
3. Chong, L., van Steensel, B., Broccoli, D., Erdjument-Bromage, H., Hanish, J., Tempst, P., and de Lange, T. (1995) *Science* **270,** 1663–1667
4. Bilaud, T., Brun, C., Ancelin, K., Koering, C. E., Laroche, T., and Gilson, E. (1997) *Nat. Genet.* **17,** 236–239
5. Broccoli, D., Smogorzewska, A., Chong, L., and de Lange, T. (1997) *Nat. Genet.* **17,** 231–235
6. Baumann, P., and Cech, T. R. (2001) *Science* **292,** 1171–1175
7. Makarov, V. L., Hirose, Y., and Langmore, J. P. (1997) *Cell* **88,** 657–666
8. Griffith, J. D., Comeau, L., Rosenfield, S., Stansel, R. M., Bianchi, A., Moss, H., and de Lange, T. (1999) *Cell* **97,** 503–514
9. Loayza, D., Parsons, H., Donigian, J., Hoke, K., and de Lange, T. (2004) *J. Biol. Chem.* **279,** 13241–13248
10. Zaug, A. J., Podell, E. R., and Cech, T. R. (2005) *Proc. Natl. Acad. Sci. U.S.A.* **102,** 10864–10869
11. Wang, F., Podell, E. R., Zaug, A. J., Yang, Y., Baciu, P., Cech, T. R., and Lei, M. (2007) *Nature* **445,** 506–510
12. Palm, W., Hockemeyer, D., Kibe, T., and de Lange, T. (2009) *Mol. Cell. Biol.* **29,** 471–482
13. Kim, S. H., Kaminker, P., and Campisi, J. (1999) *Nat. Genet.* **23,** 405–412
14. Ye, J. Z., Hockemeyer, D., Krutchinsky, A. N., Loayza, D., Hooper, S. M., Chait, B. T., and de Lange, T. (2004) *Genes Dev.* **18,** 1649–1654
15. Liu, D., Safari, A., O'Connor, M. S., Chan, D. W., Laegeler, A., Qin, J., and Songyang, Z. (2004) *Nat. Cell Biol.* **6,** 673–680

16. Houghtaling, B. R., Cuttonaro, L., Chang, W., and Smith, S. (2004) *Curr. Biol.* **14,** 1621–1631
17. Ye, J. Z., Donigian, J. R., van Overbeek, M., Loayza, D., Luo, Y., Krutchinsky, A. N., Chait, B. T., and de Lange, T. (2004) *J. Biol. Chem.* **279,** 47264–47271
18. Liu, D., O'Connor, M. S., Qin, J., and Songyang, Z. (2004) *J. Biol. Chem.* **279,** 51338–51342
19. Kim, S. H., Beausejour, C., Davalos, A. R., Kaminker, P., Heo, S. J., and Campisi, J. (2004) *J. Biol. Chem.* **279,** 43799–43804
20. Li, B., Oestreich, S., and de Lange, T. (2000) *Cell* **101,** 471–483
21. O'Connor, M. S., Safari, A., Xin, H., Liu, D., and Songyang, Z. (2006) *Proc. Natl. Acad. Sci. U.S.A.* **103,** 11874–11879
22. Celli, G. B., Denchi, E. L., and de Lange, T. (2006) *Nat. Cell Biol.* **8,** 885–890
23. Hockemeyer, D., Palm, W., Else, T., Daniels, J. P., Takai, K. K., Ye, J. Z., Keegan, C. E., de Lange, T., and Hammer, G. D. (2007) *Nat. Struct. Mol. Biol.* **14,** 754–761
24. van Steensel, B., Smogorzewska, A., and de Lange, T. (1998) *Cell* **92,** 401–413
25. Loayza, D., and de Lange, T. (2003) *Nature* **423,** 1013–1018
26. Celli, G. B., and de Lange, T. (2005) *Nat. Cell Biol.* **7,** 712–718
27. Hockemeyer, D., Daniels, J. P., Takai, H., and de Lange, T. (2006) *Cell* **126,** 63–77
28. Denchi, E. L., and de Lange, T. (2007) *Nature* **448,** 1068–1071
29. Smogorzewska, A., and de Lange, T. (2004) *Annu. Rev. Biochem.* **73,** 177–208
30. van Steensel, B., and de Lange, T. (1997) *Nature* **385,** 740–743
31. Kelleher, C., Kurth, I., and Lingner, J. (2005) *Mol. Cell. Biol.* **25,** 808–818
32. Bianchi, A., Smith, S., Chong, L., Elias, P., and de Lange, T. (1997) *EMBO J.* **16,** 1785–1794
33. Ye, J. Z., and de Lange, T. (2004) *Nat. Genet.* **36,** 618–623
34. Berger, I., Fitzgerald, D. J., and Richmond, T. J. (2004) *Nat. Biotechnol.* **22,** 1583–1587
35. Méndez, J., and Stillman, B. (2000) *Mol. Cell. Biol.* **20,** 8602–8612
36. Hockemeyer, D., Sfeir, A. J., Shay, J. W., Wright, W. E., and de Lange, T. (2005) *EMBO J.* **24,** 2667–2678
37. Karlseder, J., Smogorzewska, A., and de Lange, T. (2002) *Science* **295,** 2446–2449
38. Sfeir, A. J., Chai, W., Shay, J. W., and Wright, W. E. (2005) *Mol. Cell* **18,** 131–138
39. Herbig, U., Jobling, W. A., Chen, B. P., Chen, D. J., and Sedivy, J. M. (2004) *Mol. Cell* **14,** 501–513
40. Tommerup, H., Dousmanis, A., and de Lange, T. (1994) *Mol. Cell. Biol.* **14,** 5777–5785
41. Bryan, T. M., Englezou, A., Dunham, M. A., and Reddel, R. R. (1998) *Exp. Cell Res.* **239,** 370–378
42. Wu, J. Q., and Pollard, T. D. (2005) *Science* **310,** 310–314
43. Zhu, X. D., Küster, B., Mann, M., Petrini, J. H., and de Lange, T. (2000) *Nat. Genet.* **25,** 347–352
44. Donigian, J. R., and de Lange, T. (2007) *J. Biol. Chem.* **282,** 22662–22667
45. He, H., Multani, A. S., Cosme-Blanco, W., Tahara, H., Ma, J., Pathak, S., Deng, Y., and Chang, S. (2006) *EMBO J.* **25,** 5180–5190
46. d'Adda di Fagagna, F., Reaper, P. M., Clay-Farrace, L., Fiegler, H., Carr, P., Von Zglinicki, T., Saretzki, G., Carter, N. P., and Jackson, S. P. (2003) *Nature* **426,** 194–198
47. O'Connor, M. S., Safari, A., Liu, D., Qin, J., and Songyang, Z. (2004) *J. Biol. Chem.* **279,** 28585–28591
48. Chen, Y., Yang, Y., van Overbeek, M., Donigian, J. R., Baciu, P., de Lange, T., and Lei, M. (2008) *Science* **319,** 1092–1096
49. Xin, H., Liu, D., Wan, M., Safari, A., Kim, H., Sun, W., O'Connor, M. S., and Songyang, Z. (2007) *Nature* **445,** 559–562
50. Takai, H., Smogorzewska, A., and de Lange, T. (2003) *Curr. Biol.* **13,** 1549–1556
51. Marcand, S., Gilson, E., and Shore, D. (1997) *Science* **275,** 986–990
52. Ancelin, K., Brunori, M., Bauwens, S., Koering, C. E., Brun, C., Ricoul, M., Pommier, J. P., Sabatier, L., and Gilson, E. (2002) *Mol. Cell. Biol.* **22,** 3474–3487
53. Churikov, D., and Price, C. M. (2008) *Nat. Struct. Mol. Biol.* **15,** 79–84
54. Lei, M., Zaug, A. J., Podell, E. R., and Cech, T. R. (2005) *J. Biol. Chem.* **280,** 20449–20456

SUPPLEMENTAL FIGURE LEGENDS

Suppl. Fig. 1. Telomere length and genotyping of HeLa subclones. *A.* Genomic blot to determine the length of the telomeric restriction fragments in 24 subclones of the HeLa1.2.11 cell line. DNA in lane 11 is derived from HeLa1.3 as indicated. MWs are given in kb. *B.* Genomic blot to determine telomere length in the indicated HeLa1.2.11 subclones after several passages (P). Each passage represents approximately 4 PD. *C.* AmpFlST PCR analysis of polymorphic short tandem repeat loci in DNA from the cell lines used in this study. Alleles found for each of the 14 loci analyzed are listed.

Suppl. Fig. 2. IF for TRF2 in cells with long and short telomeres. The indicated cell lines were treated and analyzed in parallel with the exact same settings for IF for TRF2 and TRF1. Note the greater non-telomeric staining for TRF2 in cells with short telomeres (two examples of MRC5). The right hand panel represents MRC5 cells treated with TRF2sh5, demonstrating that the overall nuclear staining is due to TRF2.

Suppl. Fig. 3. Identification of TPP1 in immunoblots. *A.* Identification of the endogenous TPP1 in HeLa1.3 cells based on co-IP with transfected Flag-tagged TIN2 or POT1 (as indicated). Control: uninfected cells. Extracts from transfected cells were subjected to Flag-IP or treated with the beads and the bound proteins were detected by immunoblot with TPP1 antibody 1150. The input lanes contain 2% of the extract used for the IPs. *B.* IP controls for the experiment in (A).

Suppl. Fig. 4. Effect of cell lysates on detection of shelterin components and derivation of the detection correction factor. Quantitative immunoblotting for each of the shelterin components was executed with baculovirus-derived protein as in Figure 2. Baculovirus protein was either run alone, mixed with BSA and approximatelyl 10 μg Protein Molecular Maker (BSA+MM), or mixed into the indicated whole cell lysates (chosen to lack or have diminished representation of the endogenous protein) representing 100,000 cells. The concentrations of the baculovirus-derived proteins were determined as in Fig. 1a. Antibodies used were: TRF1, 371; TRF2, 647; Rap1, 765; TIN2, 864; TPP1, 1150; POT1, 978. Immunoblotting for POT1 was done using guanidine renaturation. The detection correction factors were derived from comparison of the signal intensities in the lanes with and without cell lysates.

Suppl. Fig. 5. Rap1 is predominantly chromatin-bound in mouse cells. Immunoblot for TRF2 and Rap1 in whole cell lysate (WC), cytoplasmic proteins (CP), nucleoplasmic proteins (NP), and chromatin-bound proteins (CB) derived from mouse NIH3T3 cells.

Suppl. Fig. 6. Knockdown of TRF2 does not affect the structure of the telomere terminus. *A.* G-strand overhang assay on HTC75 cells treated with TRF2 shRNAs or luciferase grown for the indicated PDs. Left panel: signals obtained by in-gel annealing of a labeled C-strand oligonucleotide to native digested DNA. Right panel: signal obtained by annealing the same probe to the same gel but after NaOH in situ denaturation of the DNA. *B.* Quantification of the overhang assay in (A). For each lane, the 3' overhang signal was normalized to the total

TTAGGG repeat signal. These values were then expressed compared to the value of the luciferase control PD 0 lane. *C.* Schematic of the STELA assay. *D.* STELA assay on HTC75 cells expressing luciferase sh or TRF2 sh1 or 5. C-telorettes and their cognate 5' ends as specified in (C).

Suppl. Figure 1. Takai et al.

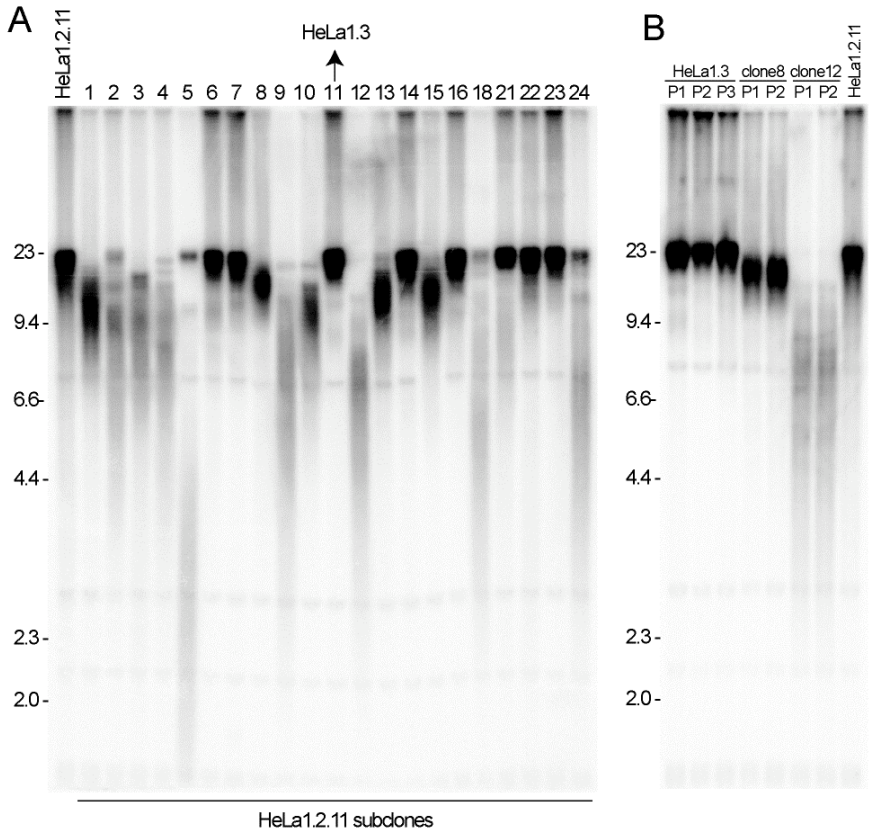

C

Locus	Alleles in HeLa1.2.11	HeLa1.3	HeLaII	HTC75
CSF1PO	9/10	9/10	9/10	12/1/2
D13S317	12/13.5	12/13.5	12/13.5	12/14
D16S539	9/10	9/10	9/10	9/12
D18S51	16/16	16/16	16/16	12/18
D19S433	13/14	13/14	13/14	13.2/15
D21S11	27/28	27/28	27/28	28/30
D2S1338	17/17	17/17	17/17	25/26
D3S1358	15/18	15/18	15/18	16/16
D5S818	11/12	11/12	11/12	11/13
D8S1179	12/13	12/13	12/13	13/14
FGA	18/21	18/21	18/21	22/25
TH01	7/7	7/7	7/7	6/6
TPOX	8/12	8/12	8/12	8/8
vWA	16/18	16/18	16/18	14/19

Suppl. Figure 2. Takai et al.

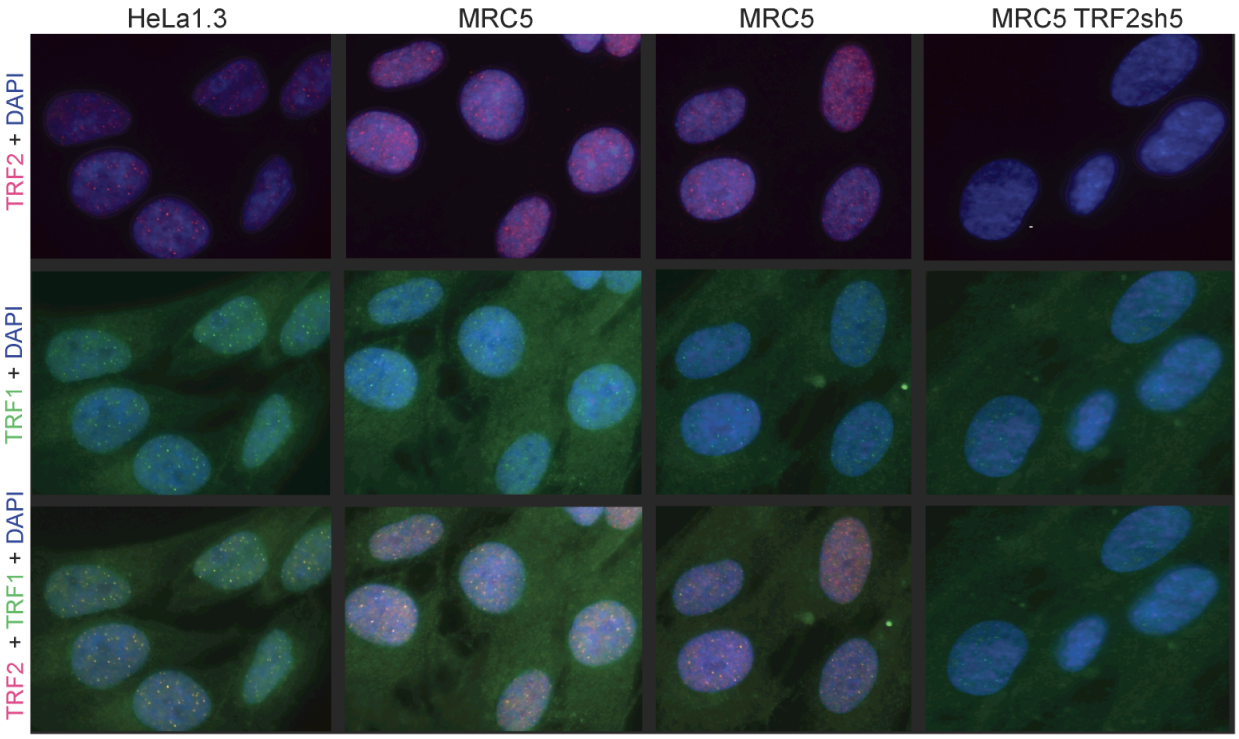

Suppl. Figure 3. Takai et al.

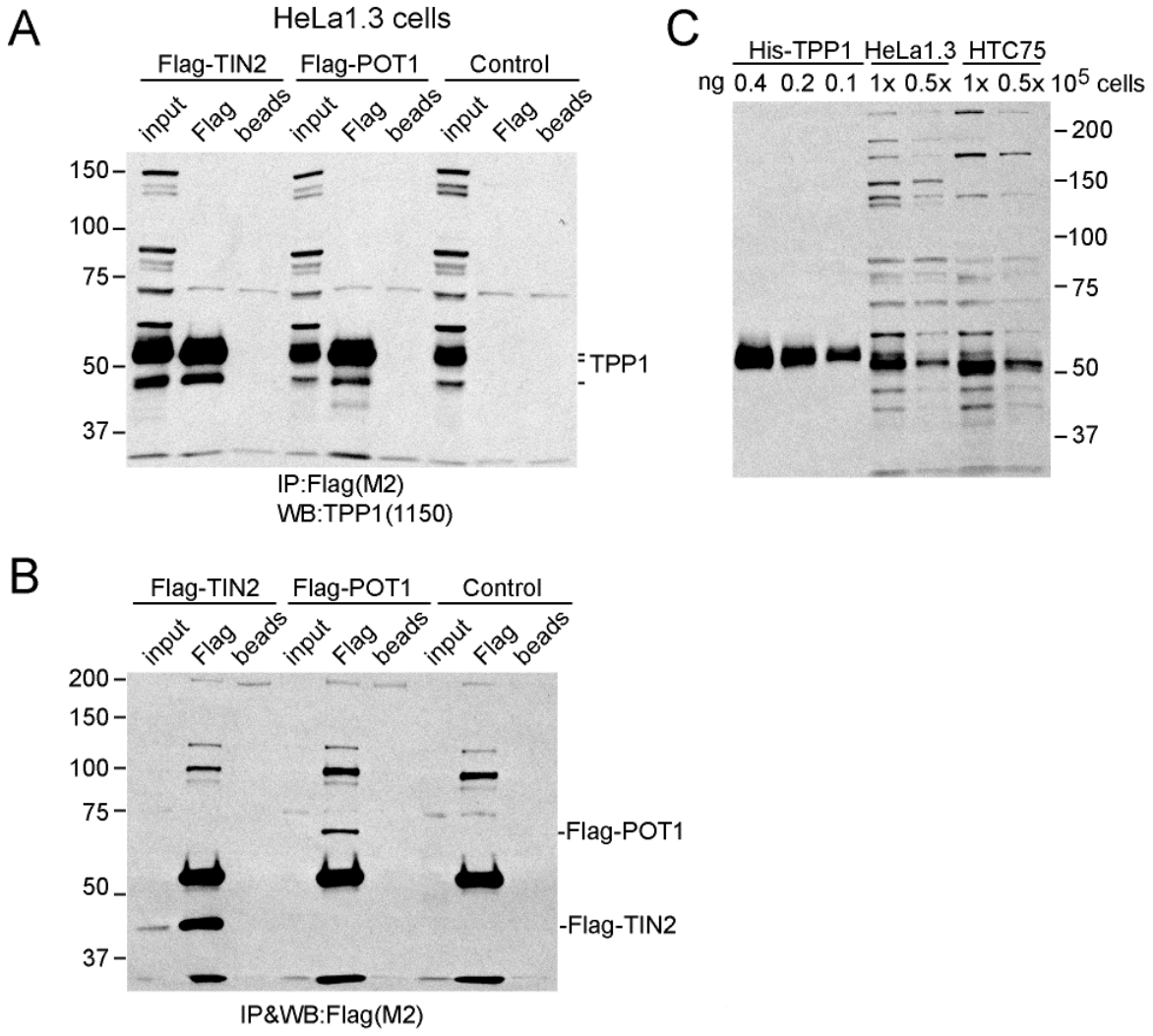

Suppl. Fig. 4. Takai et al.

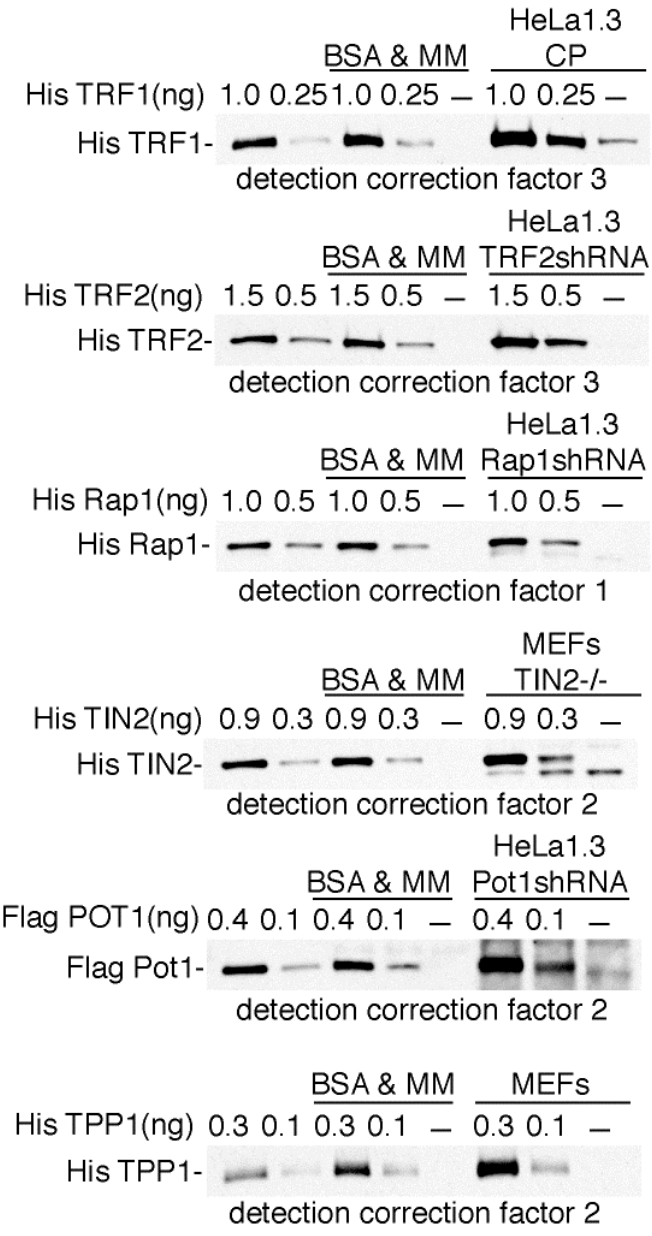

Suppl. Figure 5. Takai et al.

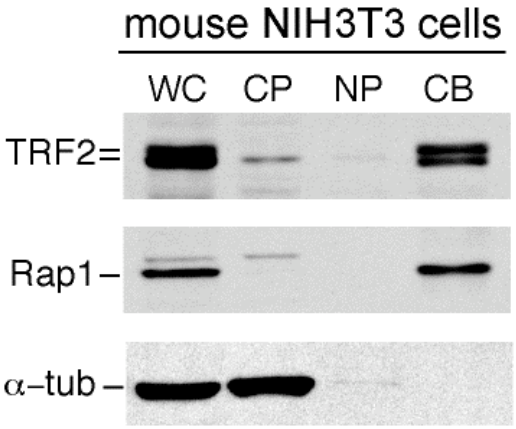

Suppl. Figure 6. Takai et al.